International Journal of Advances in Engineering and Management (IJAEM)
Volume 8, Issue 3 March. 2026, pp: 271-286 www.ijaem.net ISSN: 2395-5252

Microwave Nondestructive Evaluation Using Spiral Inductor Sensor

DanladiAgadi Tonga[1], Salisu Umar[2], Musefiu Aderinola[3], Nura Muhammed Ahmed[4], Abubakar Ahmed[5] and Lawal Kai'lu[6]

[1,3,5]Department of Electrical and Electronics Engineering Hussaini Adamu Federal Polytechnic Jigawa state Nigeria

[2,4,6] Department of Mechatronics Engineering, Hussaaini Adamu Federal Polytechnic, Kazaure, Jigawa State

Date of Submission: 13-03-2026 Date of Acceptance: 27-03-2026

Abstract—Nondestructive testing (NDT) techniques play a critical role in assessing structural integrity across a wide range of engineering and industrial applications. This research introduces a novel approach for microwave-based nondestructive evaluation using a spiral inductor (SI) sensor. The study encompasses the design, fabrication, and characterization of the proposed sensor, which operates within a frequency range of 300 MHz to 1 GHz.The proposed SI sensor features a single-port configuration with an 8-turn square spiral geometry and a miniaturized loop antenna for electromagnetic simulation. Its performance was rigorously evaluated through a combination of numerical simulations, experimental measurements, and mathematical validation. Simulation results indicate that the sensor resonates at 530 MHz with a return loss of −34 dB, while the fabricated prototype exhibits a resonant frequency of 531 MHz with a measured return loss of −23 dB. The close agreement between simulated and measured results confirms the reliability of the design methodology and the accuracy of the fabrication process.The sensor demonstrates high sensitivity and excellent spatial resolution, making it a strong candidate for detecting and characterizing defects in conductive materials. Its performance advantages are further highlighted through comparative analysis with previously reported designs, showing improvements in resolution, sensitivity, and overall effectiveness. Additionally, the sensor offers practical benefits, including a compact design and cost-effective implementation, which enhance its potential for widespread application in industrial nondestructive evaluation scenarios.The results indicate that the proposed 8-turn SI sensor represents a significant advancement in microwave-based NDT, combining high performance with practical feasibility. Its validated design and superior sensing capabilities make it well-suited for precise defect detection and structural assessment in conductive materials.

I. INTRODUCTION

Nondestructive testing (NDT) techniques are crucial in numerous civil and military applications for identifying and evaluating potential defects. Nevertheless, the process is often complex and challenging. This complexity necessitates continuously developing innovative and effective NDT methods to improve defect detection and optimize the performance to evaluate defects in composite materials. Conventional NDT approaches, such as ultrasonic [1], x-ray[2], and thermography[3], have been extensively employed to assess the structural health integrity of various materials, including conductive materials. However, these traditional techniques must be improved when inspecting and evaluating conductive materials. Microwave imaging methods have garnered significant attention for examining low-loss composites and detecting surface cracks [4]. Near-field imaging exhibits promising potential. These approaches are increasingly gaining attention as alternatives to conventional NDT techniques, including ultrasonic phased array inspection and metal surface defect detection [5] and evaluating low-loss dielectric materials [6].

In recent decades, near-field microwave imaging probes have undergone substantial advancements, primarily focused on[7] improving their lateral resolution and sensitivity. Diverse types of probes, such as coaxial evaluation [8] waveguide-fed aperture [9], aperture probes with resonant structures [10][11], and printed planar imaging probes [12][13], have been specifically developed to detect defects. To effectively identify polarized defects like cracks and delamination, these probes must possess high sensitivity, irrespective of the defect's orientation[14]. Robust near-field microwave imaging involves using an imaging sensor to illuminate a nearby defect of interest, resulting in a disturbance in the electromagnetic field distribution around the probe. This disturbance, in return, alters the analyzed resonance frequency and complex reflection coefficient. Microwave imaging techniques for near-field applications can be broadly categorized as resonant and non-resonant. As explained in [15], resonant techniques employ specialized sensors operating within a narrow frequency band centred around their resonance frequency. These methods rely on the interaction between the resonant sensor and the defect under examination, which is influenced by changes in the sensor's resonance frequency.

In contrast, non-resonant techniques, as described in [16][17], use sensors that can operate across a broader range of frequencies and do not depend on resonance as their primary detection mechanism. Open-ended rectangular waveguides have been the favoured choice for most non-resonant near-field microwave imaging techniques [18] due to their simplicity, cost-effectiveness, and ease of fabrication. However, open-ended waveguide probes have limitations, as they typically provide resolutions in the millimetre range and require high-frequency bands operation, such as x-bands and above. Unfortunately, these high frequencies reduce signal penetration into the test sample, limiting the sensor's effectiveness in imaging low-loss materials. Moreover, the cost and complexity of the imaging system escalate with increasing frequency. While reducing the operating frequency can enhance analysis precision, it may come at the expense of image resolution. Previous research has demonstrated that near-field imaging can overcome these challenges using spiral resonators, which incorporate resonance properties like split-ring resonators into the waveguide aperture [19]and planar microwave resonators [20]. The resonator's size determines the resolution of near-field imaging with planar microwave resonators[21]. These sensors are typically constructed using microstrip lines or coplanar waveguides and rely on a two-port system to image the test sample. This study introduces a single-port sensor for near-field imaging operating in the 300MHz-1GHz frequency range, comprising a miniature loop loaded with spiral resonators (SR).

The proposed SI sensor is evaluated, and its sensitivity and resolution are investigated through simulation using CST Microwave Studio. The simulation results are validated by measuring a fabricated prototype of the sensor operating at 530MHz. This sensor's practical application is for detecting defects in conductive materials, and its effectiveness is compared with other previous relevant works. The structure of this article is as follows: Section 1 provides an introduction. Section 2 Design of the SI sensor. Section 3 presents the results and discussion. Section 4 concludes and outlines directions for further research.

Contributions: This work's new SI sensor ensures material structural integrity with excellent sensitivity and resolution in microwave nondestructive evaluation (NDE). It is appropriate for various applications due to its single-port architecture, which lowers expenses and complexity.

II. Review of previous works

This section discusses recent research by different researchers. The study in Table 1 shows the development of the spiral resonator's technique, especially highlighting sensor substrate types, probe side length dimensions, resonance frequencies, return loss, and their advantages and disadvantages.

Table 1. Comparison between related works

Ref	Substrate type	The side length of the sensor (mm)	Resonance frequency (MHz)	Return loss S11 (dB)	Advantages	Disadvantages
[22]	Roger 4530C	7.2 x 7.2	433	-28	High sensitivity, low intricate and low cost	Longer inspection period due to tiny footprint
[23]	Roger 4530C	7.0 x 7.0	420	-25	High-resolution, subsurface defect detection	Use of 2 ports, which resulted in an increased cost of sensor
[24]	Roger 4530C	7.2 x 7.2	401	-18	High resolution, Q-factor for near-field imaging	Longer duration of inspection due to small footprint
[25]	Roger 4530C	7.2 x 7.2	508	-20	Superior sensitivity, high resolution, one-	Miniaturization footprint leads to a

					port	long evaluation time
[26]	FR4	8.1 x 8.1	530	-29	High resolution	Long duration inspection
[26]	FR4	7.1 x 7.1	630	-27	High sensitivity in detecting a polarized defect	The inspection period is long due to the tiny footprint
[26]	FR4	6.1 x 6.1	783	-22	Low fabrication cost	Evaluation time is long due to the small footprint
[27]	FR4	6.0 x 6.0	741	-20	Sensitivity to lower permittivity materials, direct evaluation of low loss oil permittivity	Longer assessment period due to the small footprint
[28]	Roger 4530C	7.2 x 7.2	426	-19	Good spatial resolution, low loss	Longer examination period due to small footprint
Proposed work	FR4	10.9 x 10.9	530	-34	Improve sensitivity and resolution of 1-port probe.	-

Compared to previous related studies, the newly proposed SI sensor exhibits resonance at 530MHz with significantly improved return loss, as depicted in Table 1. This enhanced performance in return loss can be attributed to specific design parameters, including a side length of 10.9 x 10.9mm, diverse widths of inductors, and an interspacing of 0.25mm. It is worth noting that most earlier studies employed probes with additional side length, uniform width, and interspacing of 127µm. However, probes with this width and interspacing offer advantages regarding signal-to-noise ratio and output voltage linearity. In contrast, the proposed sensor, with its distinct side lengths, width, and interspacing of 10.9 x 10.9mm and 0.25mm, exhibits heightened sensitivity to external magnetic fields compared to previous research. As a result, broader spiral inductors with increased interspacing demonstrate superior performance in sensitivity and accuracy, providing a larger surface area for detecting defects arising from alterations in the magnetic field. This research contributes to nondestructive testing, particularly the evaluation of conductive materials. It adds value to the field by introducing a novel sensor with increased sensitivity and resolution. The research's results, substantiated through simulations, measurements, and mathematical validations, highlight the significance of microwave nondestructive evaluation. The subsequent section provides a detailed design methodology of the sensors.

DESIGN OF SPIRAL INDUCTOR SENSORS

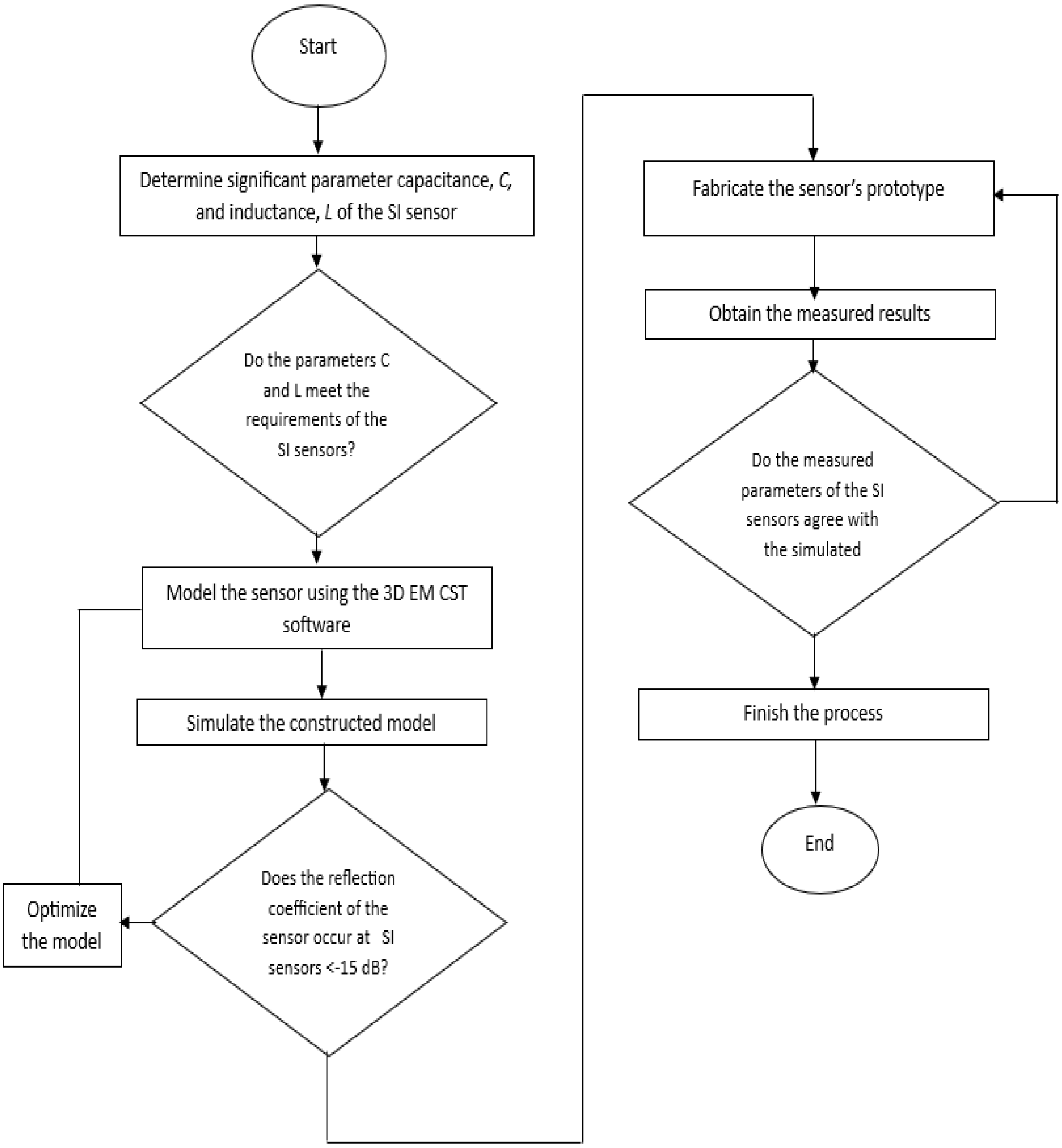

Figure 1. Flow chart design procedures of SI sensors.

The methodology used to realize the proposed sensor is outlined sequentially, with each step contributing to the overall flow of the process. The flow chart in Figure 1 describes the comprehensive steps taken to produce the SI sensors.

The initial stage focuses on key design considerations, including selecting materials and determining parameters. The materials chosen for the sensors include an FR4 substrate, copper conductors, and lumped elements for circuit matching. While some parameters were predefined, others were derived through mathematical evaluation as outlined[29].

Accurate modeling of the proposed SI sensor design requires carefully establishing critical parameters. These parameters encompass the number of turns (N), the width of the turns (w), the spacing of the turns (s), the external diameter (d_{out}), and the internal diameter (d_{in}).The design parameters for the sensor were determined using standard formulae for inductance, capacitance, and resonant frequency, as expressed in equations (1)-(3)[30][31]. This ensures the design's precision and functionality.

For the inductance of the L^{SR} is given by equation

$$L^{SR} = \frac{\mu_0}{2\pi}\ell^{SR}_{avg}\left[in\left(\frac{\ell^{SR}_{avg}}{2\omega}\right) + \frac{1}{2}\right] \quad (1)$$

Also, for the capacitance of the SI sensor C^{SR} is expressed as follows

$$C^{SR}\frac{\ell}{4(s+\omega)}\frac{N^2}{N^2+1}\left[\ell(N-1) - \frac{N^2-1}{2}(\omega+s)\right]C_0 \quad (2)$$

Here, ℓ represents the side length of the outermost turn, ωdenotes the strip widths, s is the spacing between turns, N is the total number of spiral turns, C_0 correspond to the multiple split-ring resonators and $\ell^{SR}_{avg} = 4\ell - \left[2(N+1) - \frac{3}{N}\right](\omega + s)$ is the average length of the spiral turn.

The resonant frequency of the spiral inductor sensor can be calculated using the following expression:

$$F_{resonant} = \frac{1}{\sqrt[2\pi]{\left(L_{spiral} \times C_{spiral}\right)}} \quad (3)$$

After the design phase, the sensor was simulated with electromagnetic numerical software CST MW studio 2021. During the simulation, the SI sensor resonates at a frequency of 530MHz with a return loss below -15dB, revealing its sensitivity and functionality. If the simulated return loss meets this threshold, the design proceeds to the next stage. Otherwise, the design is refined and re-simulated until the desired performance is achieved. The finalized simulation results were exported as a DXF file for fabrication. The DXF file is generated using Corel Draw software, ensuring compatibility with fabrication.

The fabrication begins with printing the circuit board and then laminating it using a photoresist dry film machine. Next, the laminated board is exposed using an exposing machine to eliminate the lamination. A conveyorized sprayer developer then removes the remaining photoresist dry film. Subsequently, the copper components of the PCB were selectively etched, leaving only the PCB and the spiral SI. The sample is immersed in a stripper solution to eliminate residual photoresist dry film. Finally, the sample is thoroughly dried utilizing a blower. The final assembly of the prototypes involves soldering SMA connectors and lumped elements onto the circuit board. The assembled prototypes were evaluated in a controlled environment using a performance network analyzer (PNA-XN5245A). If the measured results deviate significantly from the simulation outcomes, the design and assembly process is iteratively refined until the results achieve satisfactory alignment.

Figures 2 (a) 4- turn, (b) 6- turn, (c) 8- turn, (d) 10- turn, and (e) 12- turn present the simulated and fabricated of different numbers of SI sensors.

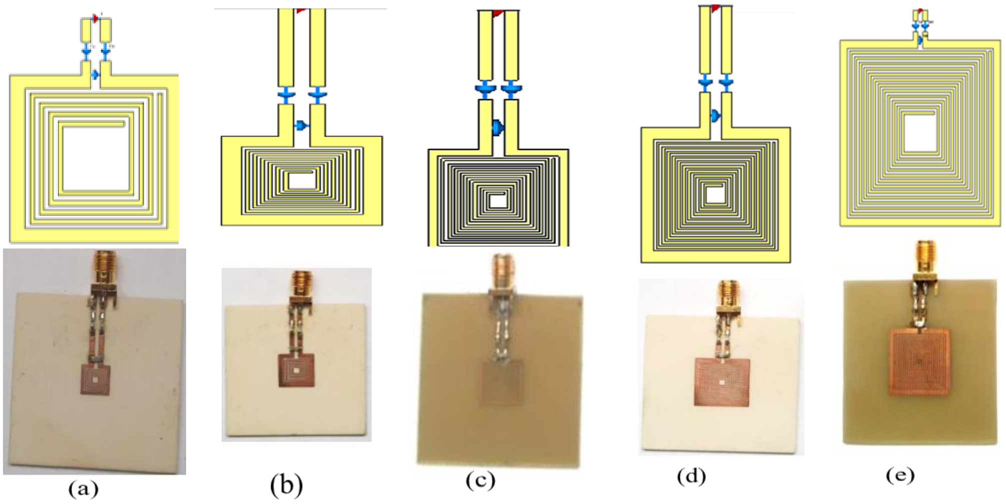

Fig. 2(a) 4-turn, (b) 6-turn, (c) 8-turn, (d) 10-turn and (e) 12-turns simulated and fabricated SI sensors

This sequential approach outlines the systematic progression from design through simulation, fabrication, prototype assembling, and final measurement, ensuring the quality and functionality of the SI sensor. Figures 3 present (a) 3D SI sensor model2(b) return loss in dB, showing the sensor's performance, while Table 2 presented the designed parameters.The next section of this paper presents the results of the proposed sensor prototypes and discusses them.

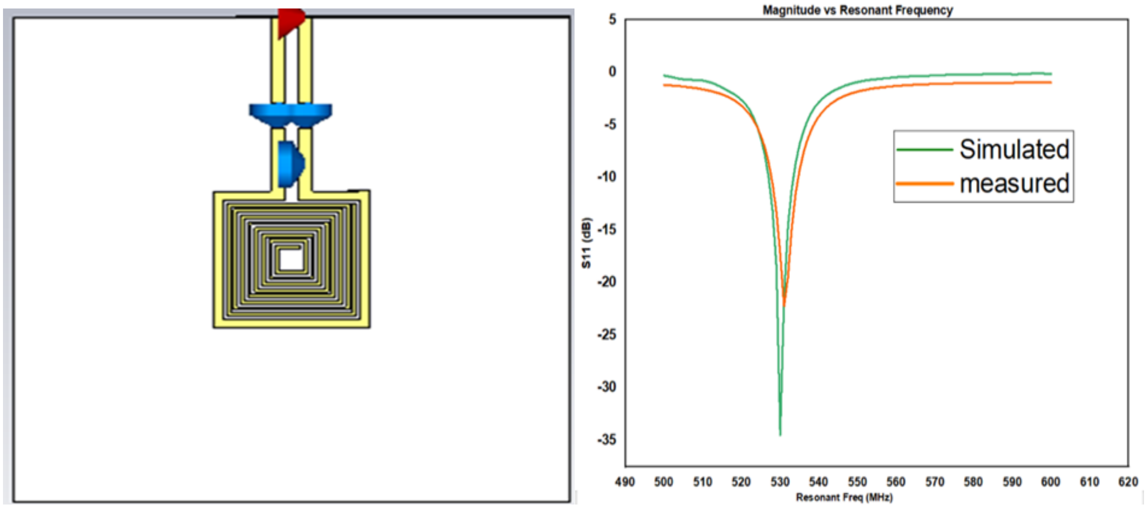

(a) (b)

Figure 3. Show (a) 3D SI Sensor model and (b) return loss of SI sensor performance.

Table 2. Designed parameters of SI sensors.

S/No	Parameter	Value (mm)
1	The permittivity of the FR4 substrate	4.3
2	The tangent loss of the FR4 substrate	0.025
3	Printed circuit board (PCB) substrate thickness	1.6
4	Thickness of Copper	0.035
5	SR conductor width of the sensor	0.25
6	Spacing between strip conductors	0.25

III. RESULTS AND DISCUSSION

This section discusses the sensor's performance, focusing on its characterization, sensitivity, resolution evaluation, fabrication,and measurement.

Spiral Inductor Sensor Characterization

The study systematically evaluated the performance of spiral inductor (SI) sensors with varying numbers of turns by integrating electromagnetic numerical simulations, theoretical modelling, and experimental measurements of the fabricated prototypes. Electromagnetic simulations were performed using CST Microwave Studio to analyze the resonant characteristics and return loss behaviour of each sensor configuration. Experimental validation was conducted using a Keysight N5245A PNA-X Performance Network Analyzer to measure the input return loss (S11) at the 50-Ω feed terminal of each fabricated sensor. To achieve optimal sensor performance, impedance matching and resonance tuning were implemented by incorporating a variable capacitor (Cm) with a capacitance range of 5–12 pF. This tuning process was carried out to minimize the return loss and to align the measured resonant frequency with the designed operating frequency of the sensors.

The comparative performance of the SI sensors was analyzed through graphical representations of the return loss (in dB) obtained from simulation, theoretical estimation, and experimental measurements. Under free-space testing conditions, the fabricated sensors exhibited resonant frequencies of 419 MHz, 362 MHz, 531 MHz, 495 MHz, and 358 MHz for the respective turn configurations. These experimental results showed good agreement with the simulated resonant frequencies of 410 MHz, 386 MHz, 530 MHz, 442 MHz, and 358 MHz. Furthermore, the theoretically calculated resonant frequencies were 400 MHz, 335

MHz, 540 MHz, 375 MHz, and 360.39 MHz, respectively. The close correlation among simulation, theoretical prediction, and experimental measurements confirms the reliability of the design methodology and validates the electromagnetic modelling approach used for sensor optimization.

Among the evaluated configurations, the 8-turn SI sensor demonstrated the most favourable performance characteristics. This sensor resonated at approximately 530 MHz and achieved a significantly low return loss of −34 dB, indicating strong impedance matching and efficient electromagnetic coupling. The improved return loss suggests higher sensitivity to perturbations in the electromagnetic field, which is essential for accurate defect detection in conductive materials. The enhanced sensitivity of the 8-turn configuration can be attributed to the optimized balance between inductance, distributed capacitance, and electromagnetic field concentration, which collectively influence the sensor's resonance behaviour and detection capability.

Based on these performance characteristics, the 8-turn SI sensor was selected for further investigation and application in defect characterization. Its superior sensitivity and stable resonance response make it particularly suitable for detecting and quantifying surface defects, including the estimation of crack location, width, and depth in conductive materials. The subsequent section presents a detailed analysis and discussion of the performance characteristics of each SI sensor configuration, highlighting the influence of geometric parameters on resonant behaviour and sensing capability.

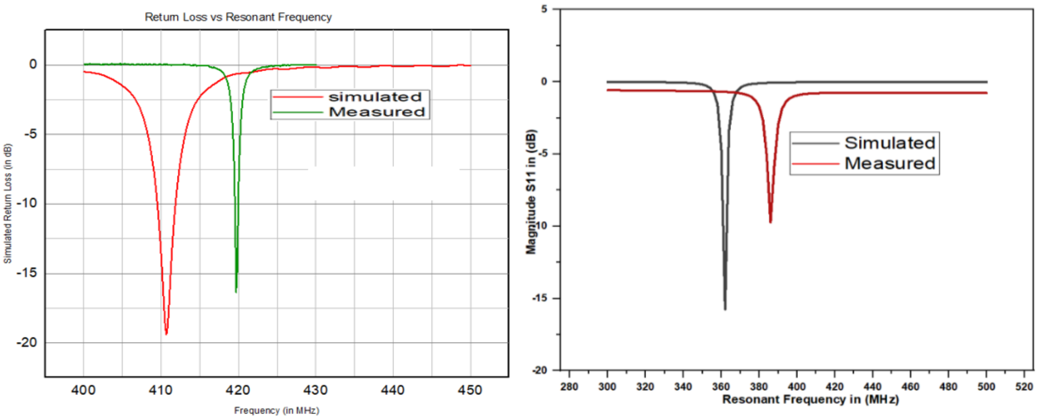

(a) (b)

Figure 4. Compared the performance of simulated and measured (a) 4-turns and (b) 6-turns SI sensors

Figures 4(a) and 4(b) illustrate the performance characteristics of the 4-turn and 6-turn spiral inductor (SI) sensors, respectively, highlighting the comparison between simulated and experimentally measured results. The electromagnetic simulations were carried out using CST Microwave Studio, while the experimental measurements were obtained using a Keysight N5245A PNA-X Performance Network Analyzer to evaluate the input return loss (S11) at the 50-Ω feed terminal of the fabricated sensor prototypes.

For the 4-turn SI sensor, the results demonstrate a strong agreement between simulation and experimental measurements. The simulated response indicates that the sensor resonates at approximately 410 MHz with a return loss of −19 dB, while the measured result shows a resonant frequency of 419 MHz with a return loss of −17 dB. The close correspondence between the simulated and measured responses confirms the accuracy of the electromagnetic modelling and the effectiveness of the sensor fabrication process. The relatively low return loss observed in both results indicates acceptable impedance matching and stable resonant behaviour, which are important characteristics for reliable sensing applications.

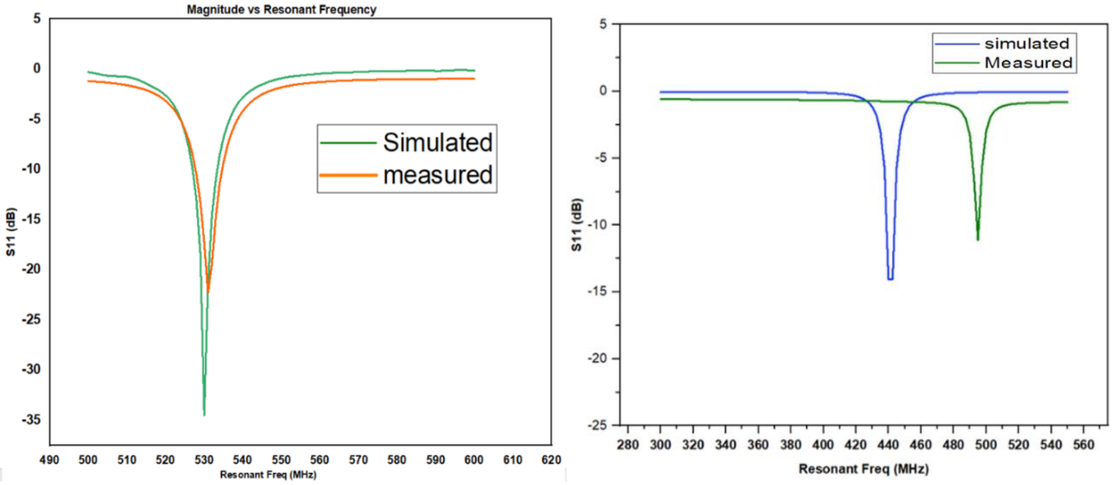

(a) (b)

Figure 5. Comparisons simulation and measurement of the (a) 8-turns, (b) 10-turns SI sensors.

Similarly, Figures 5(a) and 5(b) present the simulated and measured performance characteristics of the 8-turn and 10-turn spiral inductor (SI) sensors, respectively. The electromagnetic responses of these sensors were analyzed through numerical simulations conducted using CST Microwave Studio, while the experimental measurements were obtained using a Keysight N5245A PNA-X Performance Network Analyzer to evaluate the input return loss (S11) at the 50-Ω feed terminal of the fabricated sensor prototypes.Figure 5(a) illustrates the performance of the 8-turn SI sensor, which demonstrates the most favourable characteristics among the evaluated configurations. The simulated and measured responses exhibit a strong correlation, indicating a high level of agreement between the designed and fabricated sensor. The simulation results show that the sensor resonates at approximately 530 MHz with a return loss of −34 dB, indicating excellent impedance matching and strong electromagnetic coupling at resonance. Correspondingly, the fabricated prototype resonates at approximately 531 MHz with a measured return loss of −22.20 dB. The minimal shift in resonant frequency between the simulated and measured results confirms the robustness of the design and the reliability of the fabrication process. The slightly higher return loss observed in the experimental measurement may be attributed to practical factors such as fabrication tolerances, connector losses, and minor parasitic effects introduced during soldering and assembly.The superior performance of the 8-turn SI sensor suggests that this configuration provides an optimal balance between inductance, distributed capacitance, and electromagnetic field confinement within the spiral structure. This balance enhances the interaction between the sensors near electromagnetic field and the test material, thereby improving sensitivity to variations in the electromagnetic properties of conductive surfaces. Consequently, the 8-turn configuration offers improved sensing capability and spatial resolution compared with sensors having fewer turns. The enhanced performance also aligns with observations reported in related studies summarized in Table 1, where optimized spiral geometries have been shown to improve defect detection sensitivity in microwave-based sensing applications.

Figure 5(b) presents the performance characteristics of the 10-turn SI sensor. The results indicate that the simulated resonant frequency occurs at approximately 442 MHz with a return loss of −14.06 dB. In contrast, the experimental measurement shows that the fabricated sensor resonates at approximately 495 MHz with a return loss of −11.13 dB. Although a moderate shift in resonant frequency is observed between the simulated and measured responses, the overall resonant behaviour remains consistent. Such variations are typically associated with practical fabrication and assembly factors, including slight deviations in spiral trace dimensions, variations in substrate dielectric properties, and parasitic capacitances introduced by the SMA connector and soldering interface.Furthermore, the increase in the number of turns in the spiral structure leads to a higher inductance and stronger electromagnetic field confinement within the sensor geometry. While this can enhance field interaction with the test material, excessive turns may also introduce additional parasitic capacitance and conductor losses, which can slightly degrade impedance matching and reduce the magnitude of the return loss. This effect explains the comparatively lower return loss observed for the 10-turn sensor relative to the 8-turn configuration.Overall, the comparative analysis of the 8-turn and 10-turn SI sensors demonstrates that the 8-turn configuration provides the most balanced performance in terms of resonant stability, return loss magnitude, and sensing capability. These characteristics make it a suitable candidate for high-sensitivity applications such as crack detection and defect characterization in conductive materials. Microwave sensing applications and provide a foundation for further optimization and performance analysis of sensors with higher turn numbers.

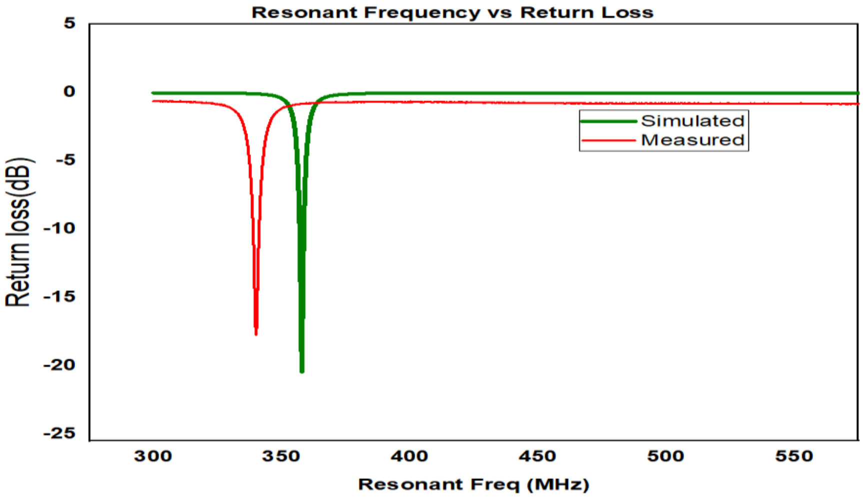

Figure 6. The comparison of the simulated and measured performance of the 12-turn SI sensor operating with the frequency range of 300 MHz to 550 MHz

Figure 6 shows a comparison performance of the simulation and measurement results for the 12-turnSI sensor configuration. The results achieved show a centre frequency of 358.85MHz and 379MHz for the simulated and measurement performance achieving the return losses of -20.43dB and -17.72 dB, respectively.

Table 3. Result comparison

S/No	Number of Turns	Simulated Resonant Frequency (MHz)	Measured Resonant Frequency (MHz)	Calculated Resonant Frequency (MHz)
1	4	410.00	419.70	400.00
2	6	386.00	362.00	335.00
3	8	530.00	531.00	540.00
4	10	442.00	495.00	375.00
5	12	358.85	340.00	360.39

Table 3 summarizes the comparative results obtained from electromagnetic simulation, experimental measurement, and mathematical validation for the spiral inductor (SI) sensors with different numbers of turns. The simulation analysis was performed using CST Microwave Studio, while the experimental measurements were carried out using a Keysight N5245A PNA-X Performance Network Analyzer to determine the input return loss (S11) and resonant frequency of each fabricated sensor. The table provides a comprehensive comparison of the resonant frequencies obtained from the three evaluation approaches, enabling a detailed assessment of the consistency and reliability of the sensor design methodology.

From the results presented in Table 3, it can be observed that slight variations exist between the simulated, measured, and mathematically validated resonant frequencies for each SI sensor configuration. Although the overall trends remain consistent, the magnitude of the frequency shifts differs among the sensors. These discrepancies can be attributed to several practical factors commonly encountered in microwave sensor fabrication and testing. For instance, tolerances associated with printed circuit board (PCB) manufacturing may introduce small deviations in the geometric dimensions of the spiral traces, such as line width, spacing, and overall lateral dimensions. In addition, variations in the dielectric properties of the substrate material can influence the effective capacitance of the resonator structure. The FR4 substrate, which is widely used in microwave circuit fabrication, often exhibits non-uniform dielectric characteristics due to manufacturing inconsistencies, leading to slight differences between simulated and measured responses.

Furthermore, the assembly process can introduce additional parasitic effects that influence the resonant behaviour of the sensors. These include imperfections during the soldering of the SMA connector, variations in the placement of discrete tuning components, and minor misalignments at the feed interface. The flexibility in selecting discrete components, such as variable capacitors used for impedance tuning, can also contribute to small variations in the measured resonant frequency. Although all SI sensors were designed using the same geometric design approach and fabricated on the same PCB substrate through identical manufacturing procedures, their physical placement on the PCB and slight dimensional differences among the spiral structures may result in distinct electromagnetic responses. Consequently, each sensor experiences unique variations between its simulated, measured, and theoretically predicted performance.

Despite these variations, the comparative results confirm that the overall design methodology remains valid, as the simulated and experimental results demonstrate reasonable agreement across all sensor configurations. Among the evaluated designs, the 8-turn SI sensor exhibits the most favourable performance characteristics, showing excellent resonance stability and a significantly lower return loss compared with the other configurations. This superior performance indicates stronger impedance matching and enhanced electromagnetic field interaction, which are essential for achieving high sensitivity in defect detection applications. For this reason, the 8-turn SI sensor was selected as the optimal configuration for further investigation in the detection and characterization of defects in conductive materials.

In general, the observed trend in resonant frequency aligns with the expected behaviour of planar spiral resonators, where the resonant frequency typically increases as the lateral dimensions of the resonator decrease. This phenomenon occurs because a reduction in the spiral size leads to a decrease in both the effective inductance and distributed capacitance of the structure, thereby increasing the self-resonant frequency of the sensor. However, the 8-turn and 10-turn SI sensors do not strictly follow this general trend due to differences in their inner diameters and geometric configurations. These structural variations alter the distribution of inductance and capacitance within the spiral, resulting in slight deviations from the expected scaling behaviour.

In contrast, the 4-turn, 6-turn, and 12-turn SI sensors generally exhibit the anticipated trend, where variations in lateral dimensions lead to corresponding increases or decreases in the resonant frequency. The reduction in the side length of the SI sensor decreases the overall inductive path and distributed capacitance, which consequently shifts the resonant frequency to a higher value. This behaviour is consistent with the theoretical principles governing spiral resonator structures in microwave sensing applications.

Based on these observations, the performance of the SI sensors will be further evaluated in terms of sensing sensitivity and spatial resolution. These parameters are critical for determining the capability of the optimized sensor configuration to accurately detect and characterize surface defects, including the location, width, and depth of cracks in conductive materials. The subsequent analysis therefore focuses on quantifying these sensing characteristics to establish the suitability of the proposed SI sensor for high-resolution non-destructive testing applications.

Evaluation of Spiral Inductor Sensor Resolution and Sensitivity

The imaging capability of the spiral inductor (SI) sensor is strongly influenced by the spatial distribution of electromagnetic fields within its near-field region. In near-field sensing applications, the concentration and confinement of electromagnetic energy around the sensing structure play a critical role in determining the sensor’s sensitivity and spatial resolution. A well-confined near-field enables stronger interaction between the electromagnetic field and the surface of the inspected material, thereby improving the sensor’s ability to detect small variations caused by surface defects such as cracks or discontinuities in conductive materials.

To analyze this behaviour, an electromagnetic numerical simulation approach was employed to investigate the near-field radiation characteristics of the SI sensor. The simulations were performed using CST Microwave Studio, which allows detailed visualization and evaluation of electromagnetic field distributions around the sensing structure. The analysis primarily focused on evaluating the magnitude and spatial distribution of the electric field intensity, as the electric field component is particularly important in determining the interaction between the sensor and the test specimen in microwave sensing applications.

Figure 7 presents the simulated electric field distribution of the SI sensor within the near-field region. The field behaviour is examined across three orthogonal planes corresponding to the x-, y-, and z-axes of the sensor structure. This multi-axis evaluation provides a comprehensive understanding of how the electromagnetic energy is distributed around the spiral geometry and how it propagates within the immediate vicinity of the sensor surface. The results illustrate the regions of field concentration and the extent of field penetration above and around the spiral structure.

.

The analysis of these field distributions provides valuable insight into the sensing mechanism of the SI sensor. In particular, regions exhibiting strong electric field intensity indicate areas where the sensor is most sensitive to perturbations caused by defects in the test material. When a conductive surface with a crack or discontinuity is introduced into this region, the local electromagnetic field distribution is altered, which in turn modifies the resonant response and return loss characteristics of the sensor.

Therefore, understanding the near-field electric field distribution is essential for evaluating and optimizing the imaging performance of the SI sensor. The field analysis presented in Figure 7 helps to identify the effective sensing region and provides guidance for optimizing the sensor geometry to achieve improved sensitivity and spatial resolution in non-destructive evaluation (NDE) applications.

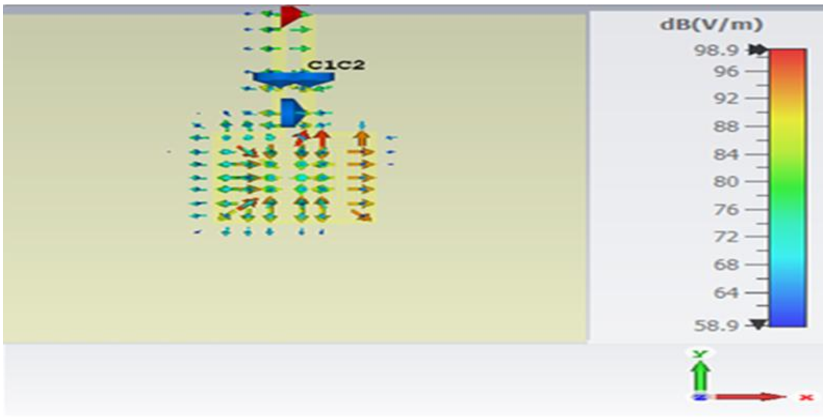

Figure 7. Electric field distribution

The sensitivity of the spiral inductor (SI) sensor is strongly influenced by the concentration and distribution of electromagnetic fields in its near-field region. Higher field intensities in the vicinity of the sensor enhance its ability to detect small perturbations caused by minor defects on conductive surfaces. The calibration scale of the simulation results indicates that the electric field (E-field) strength ranges from 98.8 dB(V/m) to 58.9 dB(V/m). Notably, the x-axis exhibits the highest concentration of the E-field, reaching 98.9 dB(V/m), which significantly improves the sensor's sensitivity for detecting fine defects. In contrast, the E-field along the y-axis decreases to 72 dB(V/m), indicating a moderate reduction in sensitivity, while the z-axis shows the lowest field strength of 58.9 dB(V/m), resulting in suboptimal performance for defect detection along this orientation. These variations demonstrate that the sensor's detection capability is anisotropic, with its highest efficiency aligned along the x-axis where field intensity is maximized.

The higher electric field values along the x-axis enable the sensor to respond more effectively to minor disruptions in the electromagnetic environment, improving detection accuracy for small defects in conductive materials. This spatial distribution highlights the importance of near-field optimization in SI sensor design, as it directly correlates with the sensitivity and reliability of defect detection.

Beyond electric field analysis, the sensor's resolution is further characterized by evaluating the magnetic energy density in the near-field region. Two-dimensional simulations were performed to map the magnetic energy distribution, which is a critical parameter for assessing spatial resolution in imaging applications. Figure 8 presents the magnetic energy density distribution, measured in dB(J/m³), showing values ranging from −14.1 dB(J/m³) to −54.1 dB(J/m³). Regions with higher magnetic energy density correspond to areas of stronger field confinement, indicating enhanced resolution capabilities. Conversely, areas with lower energy density exhibit reduced sensitivity, potentially limiting the sensor's ability to resolve fine structural details.

The combined analysis of electric field strength and magnetic energy density provides a comprehensive understanding of the SI sensor's near-field behaviour. High E-field intensity along the x-axis, coupled with localized regions of elevated magnetic energy, ensures that the sensor achieves both high sensitivity and improved spatial resolution. These characteristics make the proposed SI sensor highly suitable for non-destructive evaluation of conductive materials, particularly in applications requiring precise detection and characterization of small defects. The results demonstrate the sensor's potential to provide accurate imaging performance, guiding further optimization for defect localization and resolution enhancement in practical inspection scenarios.

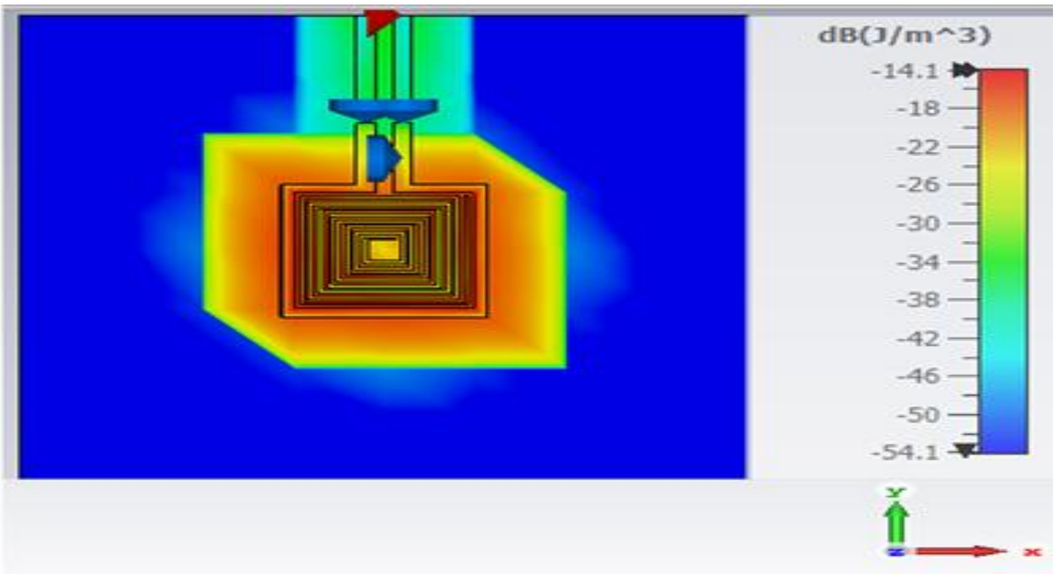

Figure 8. Magnetic energy density distribution.

The distribution of magnetic energy density in the spiral inductor (SI) sensor was systematically evaluated along the x-, y-, and z-axes to assess its impact on spatial resolution and defect detection capability. Along the x-axis, the sensor exhibits a pronounced concentration of magnetic energy density, with a peak value of −14.1 dB(J/m³), indicating a strong and well-confined magnetic field. This high magnetic energy density directly correlates with enhanced resolution, enabling the sensor to detect minor defects in conductive materials with high precision. The localized field concentration along this axis represents the region of maximum sensitivity and optimal imaging performance.

In contrast, along the y-axis, the magnetic energy density decreases to approximately −34 dB(J/m³), reflecting a reduction in field strength and a corresponding decrease in spatial resolution. In this region, the sensor demonstrates moderate sensitivity, which may limit its ability to detect finer defects compared with the x-axis. The reduced energy density introduces challenges in capturing subtle perturbations in the electromagnetic environment, indicating an anisotropic response of the sensor depending on the spatial orientation relative to the defect.

Along the z-axis, the magnetic energy density further decreases to −54.1 dB(J/m³), representing a substantially weaker magnetic field. At this lower energy level, the sensor's resolution is significantly impaired, making it effectively incapable of detecting minor defects. These observations highlight the critical role of magnetic energy density in governing the sensor's performance: higher energy density directly enhances resolution and defect detection capability, whereas lower energy density diminishes sensitivity and spatial accuracy.

The analysis demonstrates that the SI sensor's performance is intrinsically linked to the distribution of magnetic energy in its near-field region. Peak energy density along the x-axis provides optimal resolution, while decreased energy along the y- and z-axes results in progressively lower sensitivity. This understanding emphasizes the importance of near-field optimization in the design of high-resolution SI sensors.

The subsequent section presents experimental measurements of the fabricated sensor prototype, providing a detailed assessment of its real-world performance and validating the insights obtained from the simulated magnetic energy distribution.

Fabrication and Measurement of Spiral SI

The magnitude of the return loss (S11) of the fabricated spiral inductor (SI) sensor, which varies with resonant frequency in free space, was systematically characterized using the Keysight N5245A PNA-X Performance Network Analyzer. This network analyzer provides broadband measurements across a frequency range of 10 MHz to 50 GHz, enabling precise evaluation of the sensor's resonant behaviour and impedance matching. The free-space measurements reveal that the SI sensor exhibits a resonant frequency at approximately 530 MHz, with a corresponding return loss of −34 dB, indicating strong resonance and effective impedance matching.

Figures 9(a) and 9(b) illustrate the experimental setup, showing the SI sensor prototype positioned in front of the PNA analyzer. The setup ensures proper alignment and minimizes external interference during measurements. Electromagnetic simulations of the sensor were performed using CST Microwave Studio Suite to predict the resonance characteristics, while the experimental data from the PNA analyzer were processed and plotted using OriginLab, providing a direct comparison between simulated and measured results.

Figure 10 presents the measured resonant response of the SI sensor, showing a resonant frequency of 531 MHz and a minimum return loss of −23 dB. The close agreement between the simulated resonant frequency (530 MHz, −34 dB) and the measured value demonstrates the accuracy of the sensor design and the reliability of the fabrication process. The slight deviation in return loss magnitude can be attributed to practical factors such as fabrication tolerances, minor parasitic effects from the SMA connector, and substrate material inhomogeneities.

Overall, these results confirm the effectiveness of the SI sensor in achieving strong resonance and stable return loss characteristics in free-space conditions. The close correspondence between simulation and measurement validates the sensor design methodology and highlights its suitability for high-sensitivity detection of defects in conductive materials..

(a) (b)

Figure 9.(a) measurement setup, and (b) developed prototype of the SI sensor model.

The measured results exhibit a strong agreement with both the simulated responses and the mathematically validated predictions, with only minor variations observed. The slight shift in resonant frequency can be attributed to practical factors, including variations in material properties, coupling effects introduced during the soldering of the SMA connector, and the integration of surface-mounted device (SMD) lumped elements within the SI sensor. Despite these small discrepancies, the measured resonance frequency and return loss closely correspond to the simulated values, confirming the accuracy and reliability of the numerical analysis and design methodology.This strong correlation between simulation, mathematical validation, and experimental measurement demonstrates that the fabricated SI sensor performs as expected under free-space conditions and is capable of providing precise and reproducible responses for defect detection applications. The subsequent section will present the conclusions of this study and identify potential areas for future research, including optimization strategies for further enhancing sensor sensitivity, resolution, and practical applicability in non-destructive evaluation of conductive materials.

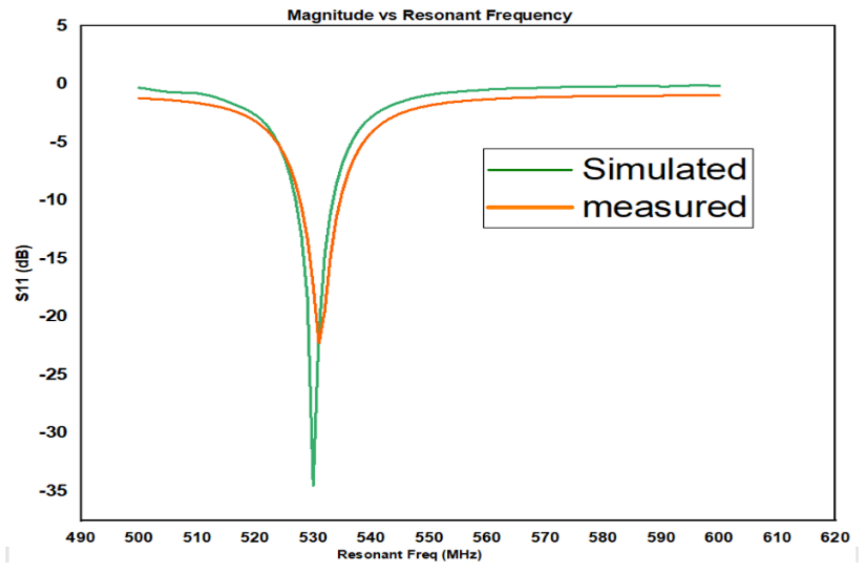

Figure 10.The Simulated and measured results of the SI sensor prototype.

IV. CONCLUSION

This study introduces an innovative microwave-based nondestructive evaluation (NDE) sensor, utilizing a spiral inductor (SI) design, for the precise assessment of defects in conductive materials. The sensor operates within the frequency range of 300 MHz to 1 GHz and demonstrates both high sensitivity and excellent spatial resolution, making it highly suitable for detecting and characterizing small surface and near-surface defects.

The research evaluates multiple SI sensor configurations with varying numbers of turns. Comprehensive electromagnetic simulations, experimental measurements, and mathematical validations were conducted for each configuration. The results show close agreement across all three approaches, with only minor variations observed due to practical fabrication tolerances, material property inconsistencies, and assembly-related effects. Among the evaluated designs, the 8-turn SI sensor exhibited the most prominent performance. The simulated results indicate a resonant frequency of 530 MHz with a return loss of −34 dB, while the measured prototype shows a resonant frequency of 531 MHz with a return loss of −23 dB. Mathematical validation further confirms the resonance at 540 MHz. This configuration achieves the highest sensitivity and spatial resolution, making it the optimal choice for defect detection in conductive materials.

The proposed 8-turn SI sensor represents a significant advancement in microwave-based NDE, offering reliable performance for high-resolution defect detection. Its design and validated performance suggest strong potential for a wide range of practical applications, particularly in the inspection of conductive components and structures. Future work should focus on further optimizing the sensor for industrial implementation, exploring its capabilities under varied operational conditions, and extending its application to more complex defect characterization scenarios in nondestructive evaluation.

REFERENCE

[1]. Yan, Y. *et al.* Non-Destructive Testing of Composite Fiber Materials With Hyperspectral Imaging - Evaluative Studies in the EU H2020 FibreEUse Project. IEEE Trans. Instrum. Meas. Vol. 71, (2022).

[2]. Rathod, H. & Gupta, R. Sub-surface simulated damage detection using Non-Destructive Testing Techniques in reinforced-concrete slabs. Constr. Build. Mater.215, 754–764 (2019).

[3]. Liu, Y., Xie, D., Zhou, R. & Zhang, Y. 3D X-ray micro-computed tomography imaging for the microarchitecture evaluation of porous metallic implants and scaffolds. Micron142, (2021).

[4]. Sepehripour, F., Alavijeh, A. S., Fakharzadeh, M. & Khavasi, A. A Broadband and Compact Millimeter-Wave Imaging System based on Synthetic Aperture Radar. (2022).

[5]. Yassin, A., Rahman, M. S. U. & Abou-Khousa, M. A. Imaging of Near-Surface Defects using Microwaves and Ultrasonic Phased Array Techniques. J. Nondestruct. Eval.37, (2018).

[6]. Abou-Khousa, M. A., Rahman, M. S. U., Donnell, K. M. & Qaseer, M. T. Al. Detection of Surface Cracks in Metals Using Microwave and Millimeter-Wave Nondestructive Testing Techniques-A Review. IEEE Trans. Instrum. Meas.72, 1–18 (2023).

[7]. Sutthaweekul, R., Tian, G. Y., Wang, Z. & Ciampa, F. Microwave open-ended waveguide for detection and characterisation of FBHs in coated GFRP pipes. Compos. Struct.225, 111080 (2019).

[8]. Dvorsky, M., Munalli, D., Qaseer, M. T. Al & Zoughi, R. Application of Microwave Polarimetry to the Characterization of Fiber Misalignment in Composites. IEEE Open J. Instrum. Meas.1, 1–9 (2022).

[9]. Malyuskin, O. & Fusco, V. Super-Resolution Defect Characterization Using Microwave Near-Field Resonance Reflectometry and Cross-correlation Image Processing. Sens. Imaging18, (2017).

[10]. Hu, B., Ren, Z., Boybay, M. S. & Ramahi, O. M. Waveguide probe loaded with split-ring resonators for crack detection in metallic surfaces. *IEEE Trans.* Microw. Theory Tech.62, 871–878 (2014).

[11]. Wang, Q. *et al.* High-Sensitivity Dielectric Resonator-Based Waveguide Sensor for Crack Detection on Metallic Surfaces. IEEE Sens. J.19, 5470–5474 (2019).

[12]. Albishi, A. M. & Ramahi, O. M. Microwaves-Based High Sensitivity Sensors for Crack Detection in Metallic Materials.IEEE Trans. Microw. Theory Tech.65, 1864–1872 (2017).

[13]. Rajni, Kaur, A. & Marwaha, A. Complementary split ring resonator based sensor for crack detection. Int. J. Electr. Comput. Eng.5, 1012–1017 (2015).

[14]. Singhwal, S. S., Kanaujia, B. K., Singh, A. & Kishor, J. Novel circularly polarized dielectric resonator antenna for microwave image sensing application. Microw. Opt. Technol. Lett.61, 1821–1827 (2019).

[15]. Abou-khousa, M. A., Member, S., Shafi, K. T. M. & Xingyu, X. High-Resolution UHF Near-Field Imaging Probe. 1–10 (2018).

[16]. Wu, R., Zhang, H., Yang, R., Chen, W. & Chen, G. Review Article Nondestructive Testing for Corrosion Evaluation of Metal under Coating. (2021).

[17]. Ghoni, R., Dollah, M., Sulaiman, A. & Mamat Ibrahim, F. Defect Characterization Based on Eddy Current Technique: Technical Review. Advances in Mechanical Engineering , (2014).

[18]. Brinker, K., Dvorsky, M., Al Qaseer, M. T. & Zoughi, R. Review of advances in microwave and millimetre-wave NDT&E: Principles and applications: Microwave and Millimeter-Wave NDT&E. *Philosophical Transactions of the Royal Society A:* Mathematical, Physical and Engineering Science*s*378, (2020).

[19]. Xie, Z. *et al.* A simple high-resolution near-field probe for microwave non-destructive test and imaging. Sensors (Switzerland*)*20, (2020).

[20]. Govind, G., Tiwari, N. K., Agrawal, K. K. & Akhtar, M. J. Microwave Subsurface Imaging of Composite Structures Using Complementary Split Ring Resonators. IEEE Sens. J.18, 7442–7449 (2018).

[21]. Ali, A., El Badawe, M. & Ramahi, O. M. Microwave Imaging of Subsurface Flaws in Coated Metallic Structures Using Complementary Split-Ring Resonators.IEEE Sens. J.16, 6890–6898 (2016).

[22]. Chuma, E. L., Iano, Y., Fontgalland, G. & Bravo Roger, L. L. Microwave sensor for liquid dielectric characterization based on metamaterial complementary split ring resonator. IEEE Sens. J.18, 9978–9983 (2018).

[23]. Memon, M. U. & Lim, S. Review of

electromagnetic-based crack sensors for metallic materials (Recent research and future perspectives). Metals6, (2016).

[24]. Zhang, C., Huthwaite, P. & Lowe, M. The Application of the Factorization Method to the Subsurface Imaging of Surface-Breaking Cracks. IEEE Trans. Ultrason. Ferroelectr. Freq. Contro*l*65, 497–512 (2018).

[25]. Sabah, C. & Nesimoglu, T. Design and characterization of a resonator-based metamaterial and its sensor application using microstrip technology. Opt. Eng.55, 027107 (2016).

[26]. Haryono, A., Aljaberi, K., Ur Rahman, M. S. & Abou-Khousa, M. A. High resolution and polarization independent microwave near-field imaging using planar resonator probes.IEEE Access8, 191421–191432 (2020).

[27]. Rahman, M. S. ur, Hassan, O. S. & Abou-Khousa, M. A. Crack Detection and Corrosion Mapping Using Loaded-Aperture Microwave Probe.IEEE Open J. Instrum. Meas.1, 1–11 (2022).

[28]. Bendaoudi, A. & Mahdjoub, Z. Comparative study of patch antenna loaded with slot split-ring resonators on different substrate materials. Photonic Netw. Commun.35, 195–203 (2018).

[29]. Bilotti, F. *et al.* Equivalent-circuit models for the design of metamaterials based on artificial magnetic inclusions. in IEEE Transactions on Microwave Theory and Techniques55, 2865–2873 (2007).

[30]. Mohan, S. S., Del Mar Hershenson, M., Boyd, S. P. & Lee, T. H. Simple Accurate Expressions for Planar Spiral Inductances. IEEE JOURNAL OF SOLID-STATE CIRCUITS34, (1999).

[31]. Buell, K., Mosallaei, H. & Sarabandi, K. A substrate for small patch antennas providing tunable miniaturization factors. IEEE Trans. Microw. Theory Tech.54, 135–145 (2006).